

TacoDepth: Towards Efficient Radar-Camera Depth Estimation with One-stage Fusion

Yiran Wang^{1,2,*} Jiaqi Li^{2,*} Chaoyi Hong^{1,2} Ruibo Li¹
 Liusheng Sun³ Xiao Song³ Zhe Wang³ Zhiguo Cao² Guosheng Lin^{1,†}

¹S-Lab, Nanyang Technological University

²School of AIA, Huazhong University of Science and Technology ³SenseTime Research

{wangyiran, zgcao}@hust.edu.cn, gslin@ntu.edu.sg

<https://github.com/RaymondWang987/TacoDepth>

Abstract

Radar-Camera depth estimation aims to predict dense and accurate metric depth by fusing input images and Radar data. Model efficiency is crucial for this task in pursuit of real-time processing on autonomous vehicles and robotic platforms. However, due to the sparsity of Radar returns, the prevailing methods adopt multi-stage frameworks with intermediate quasi-dense depth, which are time-consuming and not robust. To address these challenges, we propose TacoDepth, an efficient and accurate Radar-Camera depth estimation model with one-stage fusion. Specifically, the graph-based Radar structure extractor and the pyramid-based Radar fusion module are designed to capture and integrate the graph structures of Radar point clouds, delivering superior model efficiency and robustness without relying on the intermediate depth results. Moreover, TacoDepth can be flexible for different inference modes, providing a better balance of speed and accuracy. Extensive experiments are conducted to demonstrate the efficacy of our method. Compared with the previous state-of-the-art approach, TacoDepth improves depth accuracy and processing speed by 12.8% and 91.8%. Our work provides a new perspective on efficient Radar-Camera depth estimation.

1. Introduction

Radar-Camera depth estimation [6, 13, 21, 22, 26, 27, 29–32, 38] is a vital task for 3D perception and motion planning in autonomous driving [4, 16, 23, 50, 54] and robotics [14, 22, 40]. The task aims to predict dense metric depth by integrating images with mmWave Radar data, perceiving metric scale in different environments. As a typical range sensor on driving and robotic platforms, Radar is widely equipped and used for its high affordability and low power consump-

* Equal contribution, † Corresponding author.

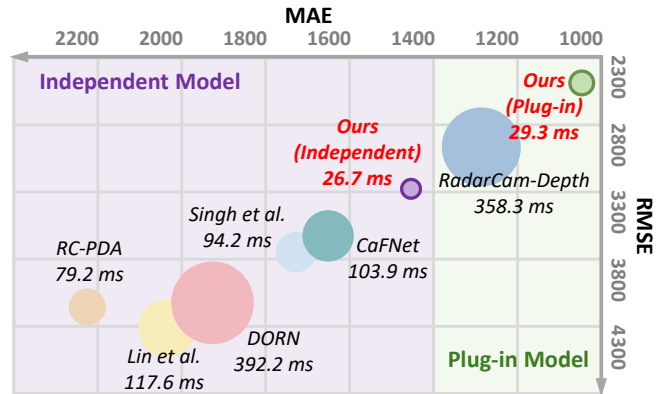


Figure 1. **Performance and efficiency.** Circle area indicates inference time (ms). Smaller circles showcase faster speed. The X-axis and Y-axis represent MAE and RMSE metrics for depth errors on the nuScenes [4] dataset. Lower MAE and RMSE mean higher accuracy. Our TacoDepth outperforms prior arts by large margins.

tion. It is valuable to explore Radar-Camera fusion in various tasks [2, 5, 9, 17, 33, 38] for its superior all-weather reliability. Besides, for real-time processing on vehicles and robotics, improving efficiency is crucial for fusion models.

The obstacle for fusing Radar in depth estimation lies in its sparsity and noises. Due to the large beam width, Radar point clouds are 1000x sparser with higher noise levels than LiDAR returns. To deal with the issue, the prevailing methods [22, 27, 29, 30, 32, 38, 39, 41] adopt complex multi-stage frameworks. Intermediate quasi-dense depth is predicted to bridge the gap between sparse Radar and final dense depth. For instance, two-stage methods [27, 29, 30, 32, 38, 39, 41] predict final depth based on intermediate results, as independent models without utilizing other depth predictors [3, 35, 36, 52]. RadarCam-Depth [22], as a plug-in module, converts relative depth [35, 36] to metric scale in four stages by post-processing. These multi-stage methods are inefficient and time-consuming, as presented in Fig. 1.

Meanwhile, despite being described as quasi-dense, the intermediate depth [22, 27, 29, 30, 32, 38, 41] remains sparse and noisy. As shown in Fig. 2, only few pixels exhibit valid depth. For some adverse lighting or weather conditions, *e.g.*, glaring and nighttime scenarios, even no pixels are predicted with depth values. These defective intermediate results lead to disrupted structures, blurred details, or noticeable artifacts in final predictions, as shown in Fig. 4. With these observations, a question naturally arises: can models directly predict accurate and dense depth without the intermediate results, achieving one-stage Radar-Camera depth estimation with higher efficiency and robustness?

To answer the above question, we propose TacoDepth, an efficient and accurate Radar-Camera depth estimation framework with one-stage fusion. To simplify multi-stage fusion [22, 27, 29, 30, 32, 38, 39, 41] into one stage, TacoDepth needs to extract and integrate Radar information more effectively. Prior arts simply extract features from Radar coordinates [22, 38] or projected depth [27, 32], sensitive to noises and outliers [12]. In contrast, we utilize a graph-based Radar structure extractor to capture geometric structures and topologies of point clouds, improving robustness to inaccurate points [12, 19, 37, 44]. After that, our pyramid-based Radar fusion module integrates image and Radar features hierarchically. Shallow layers capture image details and Radar coordinates, while deep layers fuse scene semantics and structures [10, 15, 20, 42, 46, 51]. In each layer, Radar-centered flash attention mechanism is applied to establish the cross-modal correlations. For one Radar point, lightweight and accelerated flash attention [8] is calculated within Radar-centered areas for efficiency. Finally, TacoDepth predicts accurate and dense depth by a decoder.

Moreover, we further analyze the characteristics of different inference strategies in prior arts [22, 27, 29, 30, 32, 38, 39, 41]. Independent models [27, 29, 30, 32, 38, 41] are more efficient without initial depth prediction and post-processing, while the plug-in model [22] can be more accurate by leveraging cutting-edge relative depth predictors [3, 24, 35, 52]. Therefore, TacoDepth aims to be flexible for the two settings. An auxiliary and optional branch is added for initial depth, allowing TacoDepth to support both independent and plug-in processing. Our approach can better balance depth accuracy and model efficiency.

We conduct evaluations on nuScenes [4] and ZJU-4DRadarCam [22] datasets with different depth ranges, following prior arts [22, 32, 38]. As shown in Fig. 1, whether compared with independent [27, 29, 32, 38, 41] or plug-in [22] models, TacoDepth significantly outperforms prior arts [22, 27, 29, 32, 38, 41] in accuracy and efficiency. Besides, our approach achieves real-time processing of over 37 fps as an independent model and strong compatibility with various depth predictors [3, 35, 36, 52] as a plug-in model, further proving the efficiency and flexibility of TacoDepth.

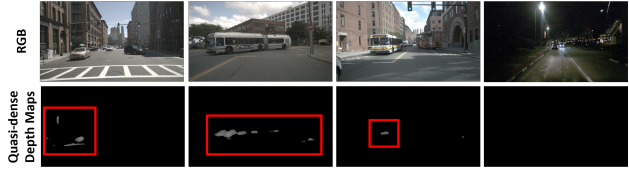


Figure 2. **Intermediate quasi-dense depth maps [22, 27, 29, 30, 32, 38, 41] remain sparse and noisy.** Pixels with valid depth values are visualized by the gray areas in the red rectangular boxes.

Our main contributions can be summarized as follows:

- We propose TacoDepth, an efficient and accurate Radar-Camera depth estimation method with one-stage fusion.
- We design the pyramid-based Radar fusion module, fusing Radar and image features effectively and efficiently.
- TacoDepth is flexible for both independent and plug-in processing, balancing model efficiency and performance.

2. Related Work

MmWave Radar for Vehicles and Robotics. Autonomous driving [4, 16, 49, 54] and robotics [14, 22, 25, 40] rely on multiple sensors to perceive the environment, *e.g.*, camera, LiDAR, and mmWave Radar. LiDAR and Radar provide the metric scale of different scenarios as a complement to cameras. Compared with LiDAR, Radar is cheaper and more widely-equipped with lower power consumption. The reflection properties of mmWave also provide Radar with farther sensing ranges and stronger robustness to all-weather conditions. The main drawback of Radar lies in its sparsity and noise. Due to the large beam width, Radar point clouds are 1000x sparser [38] than LiDAR. Besides, Radar captures coordinates and depth values with lower accuracy. For instance, 3D Radar suffers from height ambiguity [32] due to insufficient antenna elements along the elevation axis, while this problem can be alleviated by the emerging 4D Radar. Thus, integrating Radar data is valuable for various tasks [2, 5, 9, 17, 28, 33, 38] in driving and robotic systems.

Radar-Camera Depth Estimation. The task aims to predict dense metric depth by merging images and Radar, facilitating 3D perception and motion planning of vehicles and robotics. Model efficiency is crucial for these real-time applications. However, to overcome the sparsity and noise of Radar, prior arts [22, 27, 29, 30, 32, 38, 39, 41] adopt inefficient multi-stage frameworks. The final depth is predicted based on intermediate quasi-dense depth. These methods can be divided into independent and plug-in models. Most independent models [27, 29, 30, 32, 38, 41] predict final depth in two stages without relying on other depth predictors [18, 34–36, 47, 48]. For example, Lin *et al.* [27] and DORN [29] use two CNNs [15] for quasi-dense and final depth. RC-PDA [32] and RC-DPT [30] convert intermediate results into multiple channels for varied confidence levels. Singh *et al.* [38] propose gated fusion to filter the inac-

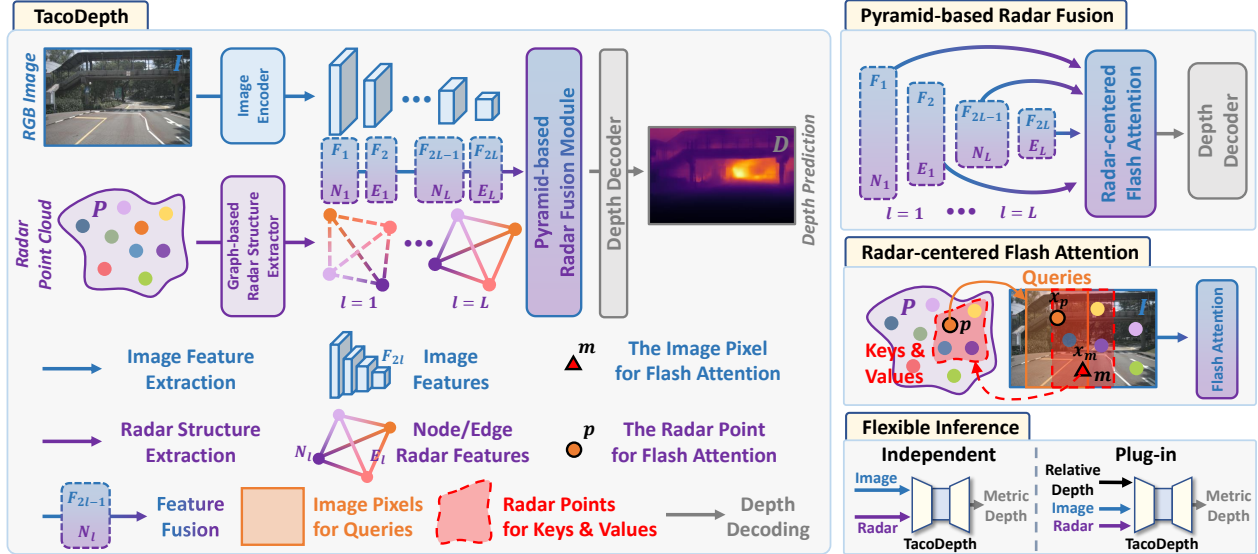


Figure 3. **Overview of the TacoDepth.** The graph-based Radar structure extractor captures graph structures of Radar point clouds through the node feature N_l and edge feature E_l in a certain layer l . The pyramid-based Radar fusion module integrates image and Radar features in a pyramidal hierarchical manner. In each layer, to efficiently build cross-modal correspondences, the Radar-centered flash attention is calculated within Radar-centered areas based on horizontal coordinates, *e.g.*, pixels in the orange area as queries, while Radar points in the red area as keys and values. Our TacoDepth achieves efficient and accurate Radar-Camera depth estimation in one stage. During inference, the model is flexible and supports both independent and plug-in processing, facilitating a better balance of model efficiency and accuracy.

curate quasi-dense depth. Besides, RadarCam-Depth [22] designs a plug-in module, aligning relative depth [35, 36] to metric scale in four stages, including initial depth, global scale alignment, quasi-dense depth, and scale learner. These methods [22, 27, 29, 30, 32, 38, 39, 41] are inefficient with complex stages. Defective intermediate depth also limits their robustness. In contrast, we propose TacoDepth model to achieve efficient, accurate, and flexible one-stage fusion.

3. TacoDepth

We present a detailed illustration of TacoDepth, an efficient Radar-Camera depth estimation framework with one-stage fusion. In Sec. 3.1, we provide an overall description to outline our approach. In Sec. 3.2, we elaborate on the detailed architecture of the pyramid-based Radar fusion module. TacoDepth can be flexible for independent and plug-in processing, which will be discussed in Sec. 3.3. Besides, the training procedure for TacoDepth is illustrated in Sec. 3.4.

3.1. Overview

Here we present an overview of our TacoDepth framework. Given a single image $I \in \mathcal{R}^{H \times W \times 3}$ and a Radar point cloud $P \in \mathcal{R}^{K \times 3}$ as inputs, our goal is to predict dense metric depth $D \in \mathcal{R}^{H \times W}$. H and W represent image height and weight. The point cloud P contains K points $p \in \mathcal{R}^3$. Radar-Camera depth estimation can be divided into two primary subtasks: the extraction and the integration of Radar information. Accordingly, as depicted in Fig. 3,

TacoDepth comprises a graph-based Radar structure extractor and a pyramid-based Radar fusion module to undertake these two important steps respectively.

Firstly, for Radar feature extraction, previous methods [22, 38] simply extract features from the coordinates of individual Radar points, focusing solely on the point-level information. For example, Singh *et al.* [38] extract point features in 32,256 dimensions from the three-dimensional coordinates using a multi-layer perceptron (MLP), which inevitably introduces substantial redundancy and noise.

To achieve efficient Radar-Camera fusion in a single stage, TacoDepth needs to extract more comprehensive and effective Radar information, prompting us to reconsider the complementarity between camera images and Radar data. Compared to the coordinates, the geometric structures of point clouds, *e.g.*, the distances or relations between Radar points, are potentially more informative for Radar-Camera fusion. The overall topologies are also more robust to inaccurate outliers [12]. To this end, we employ the graph-based Radar structure extractor with a lightweight GNN [12, 37, 44] architecture. Specifically, Radar points are regarded as the graph nodes. The adjacency matrix of all points represents the graph edges. In each layer, the node features of Radar points can be updated and aggregated along edges by PCA-GM [45]. The graph-based Radar structure extractor can capture point coordinates and graph structures from shallow layers to deep layers [12, 42, 46].

After extracting the Radar structures, the subsequent step

is to merge RGB and Radar features. Prior arts [22, 27, 29, 30, 32, 38, 39, 41] adopt multi-stage methods with intermediate quasi-dense depth, which are inefficient and not robust as illustrated in Sec. 1. In contrast, we propose our pyramid-based Radar fusion module for efficient one-stage fusion.

To be specific, features of the two modalities are integrated in a pyramidal hierarchical manner. Shallow layers can merge image details with Radar coordinates, whereas deeper layers could fuse scene semantics and geometric structures [10, 15, 20, 42, 46, 51]. In each layer, we leverage Radar-centered flash attention for cross-modal correlations and feature fusion. The queries are derived from image pixels, while keys and values originate from Radar points. For each point, we delineate Radar-centered areas based on the horizontal coordinates, as exemplified by the orange and red areas in Fig. 3, given that the projected horizontal coordinates of Radar points are generally more precise than the height dimension [32, 38]. Lightweight flash attention [8] is calculated within these areas to maintain efficiency, since external pixels and points can not be correlated. Finally, with the fused features from all layers, TacoDepth predicts accurate and dense metric depth by a depth decoder [38].

Furthermore, TacoDepth is adaptable for both independent and plug-in inference. An optional input branch is introduced to handle the initial relative depth. For the independent inference, our model achieves real-time processing of over 37 fps. For the plug-in manner, TacoDepth demonstrates compatibility with various cutting-edge depth predictors [3, 35, 36, 52], as proved in Sec. 4.5. Consequently, our approach can deliver a balanced trade-off between performance and efficiency for different users and applications.

3.2. Pyramid-based Radar Fusion

For the Radar point cloud P , our graph-based Radar structure extractor derives node feature N_l and edge feature E_l at a certain layer $l \in \{1, 2, \dots, L\}$, where L represents the layer number of the GNN module [12, 37, 44]. For the input image I , the image encoder [15, 22, 38] extracts multi-scale features $\{F_1, F_2, \dots, F_{2L}\}$. The pyramid-based Radar fusion module hierarchically integrates the multi-modal features. N_l and E_l will be fused with image features in adjacent layers. We merge the node feature N_l with image feature F_{2l-1} , and the edge feature E_l with F_{2l} , respectively.

The prerequisite for feature fusion is cross-modal correspondences between Radar points and RGB pixels. Due to the noisy elevation coordinates of 3D Radar, prior arts [22, 30, 32, 38, 41] try to build one-to-many mappings by the intermediate quasi-dense depth. They adopt explicit classification supervision with the depth discrepancies between LiDAR and Radar as pseudo-labels. However, the quasi-dense depth prediction leads to inefficiency and erroneous final outcomes, as discussed in Sec. 1. Given the absence of reliable explicit labels and supervision, we hope our TacoDepth

can learn and establish the correspondences implicitly.

Therefore, for efficient Radar-Camera correlations, we propose the Radar-centered flash attention in TacoDepth. We define Radar-centered areas based on the precise horizontal coordinates of Radar points and image pixels. For each point, the attention is computed only with image pixels in the area, since external pixels can not be correlated. Here we take $E_l \in \mathcal{R}^{K \times K}$ and $F_{2l} \in \mathcal{R}^{h \times w \times C_l}$ as examples, where h and w are feature height and width. K and C_l refer to the point number and layer feature channel. For a Radar point p with the horizontal coordinate x_p , as showcased by the exemplary orange area in Fig. 3, we only retain image pixels m whose coordinates x_m are close to x_p :

$$\hat{F}_{2l} = F_{2l} [x_p - a_l < x_m < x_p + a_l], \hat{F}_{2l} \in \mathcal{R}^{\hat{M} \times C_l}, \quad (1)$$

where a_l indicates the width of the Radar-centered area in layer l . The notation $[\cdot]$ depicts the fetching operation of pixels or points. \hat{F}_{2l} is the image feature of the remaining \hat{M} pixels to generate queries. For a random pixel m in \hat{F}_{2l} , as represented by the red area in Fig. 3, the attention calculation is also restricted to adjacent Radar points:

$$\hat{E}_l = E_l [x_m - a_l < x_p < x_m + a_l], \hat{E}_l \in \mathcal{R}^{\hat{K} \times K}. \quad (2)$$

The feature dimension maintains the original K to preserve integral graph topologies. \hat{E}_l is the edge feature of the retained \hat{K} points for keys and values. In this way, the computational costs can be significantly decreased with the small subset of \hat{M} pixels and \hat{K} points. For the pixel m , we generate queries from $\hat{F}_{2l}[m] \in \mathcal{R}^{C_l}$, while keys and values are derived from \hat{E}_l . Radar-centered attention is computed as:

$$F'_{2l}[m] = \text{softmax} \frac{W_q \hat{F}_{2l}[m] (W_k \hat{E}_l)^T}{\sqrt{C_l}} W_v \hat{E}_l, \quad (3)$$

in which W_q , W_k , and W_v are learnable linear projections. The fused Radar-Camera feature $F'_{2l} \in \mathcal{R}^{h \times w \times C_l}$ can be acquired for the current layer. The above calculation is incorporated into attention blocks with MLPs and residual connections. To further improve model efficiency, we employ lightweight and accelerated flash attention modules [7, 8] to replace the original attention computation [43].

Similarly, the node feature N_l can be merged with the image feature F_{2l-1} by slightly adjusting the dimensions of linear projections. Ultimately, the acquired Radar-Camera features $\{F'_1, F'_2, \dots, F'_{2L}\}$ are fed to a common depth decoder [22, 38] to predict accurate metric depth.

As a consequence, the proposed pyramid-based Radar fusion module enables efficient and effective Radar-Camera fusion in a single stage. The Radar-centered flash attention establishes cross-modal correlations with minimal computational costs. Without relying on the previous multi-stage frameworks and intermediate quasi-dense depth [22, 27, 29, 30, 32, 38, 39, 41], TacoDepth achieves higher efficiency and stronger robustness for Radar-Camera depth estimation.

3.3. Flexible Inference

Considering the varied inference manners in prior arts [22, 27, 29, 30, 32, 38, 39, 41], the plug-in module [22] could achieve higher accuracy using state-of-the-art relative depth predictors [35, 36, 53], while independent models [27, 29, 30, 32, 38, 39, 41] are capable of attaining faster inference speed without initial depth prediction and post-processing.

Therefore, TacoDepth is designed to be flexible, supporting both independent and plug-in predictions. For the plug-in inference, an initial relative depth map is converted to metric scale by fusing camera and Radar information. If we denote the TacoDepth model as \mathcal{T}_θ , parameterized by θ , the depth prediction process can then be formulated as follows:

$$D = \mathcal{T}_\theta(I, P | D^*), \quad (4)$$

where the vertical bar ($|$) separates the required and optional inputs. D is the predicted depth of our model. D^* is the optional input of initial relative depth from depth predictors [3, 35, 36, 52]. We introduce an auxiliary branch to process and fuse D^* with image features, while keeping all other settings identical to the independent mode. Our plug-in manner demonstrates compatibility with various depth predictors, *e.g.*, MiDaS [3, 35], DPT [36], and Depth-Anything-v2 [52]. In this way, TacoDepth can achieve a better balance of model efficiency and accuracy, offering superior flexibility for different users and applications.

3.4. Training the TacoDepth

In the training phase, the training data [4, 22] is randomly divided into two equal portions in each epoch. For the auxiliary branch, one half of the data is provided with initial relative depth, while the other half adopts zero as input. This training strategy facilitates the simultaneous optimization of the independent inference and plug-in prediction.

As for the training loss, we employ the same depth ground truth and L_1 loss as the prior art [38]. Specifically, LiDAR-captured depth D_{gt} and reprojection-accumulated depth D_{acc} are utilized for supervision [22, 32, 38]. The overall loss function ℓ_{L_1} can be expressed as follows:

$$\ell_{L_1} = \frac{1}{|\Omega_{gt}|} \sum_{\Omega_{gt}} |D - D_{gt}| + \frac{\lambda}{|\Omega_{acc}|} \sum_{\Omega_{acc}} |D - D_{acc}|, \quad (5)$$

where Ω_{gt} and Ω_{acc} depict the masks of D_{gt} and D_{acc} with valid depth values. λ is the coefficient of the second term.

4. Experiments

To prove the efficacy of our TacoDepth, we conduct experiments on the nuScenes [4] and ZJU-4DRadarCam [22] datasets following prior arts [21, 22, 27, 29, 30, 32, 38, 41]. In Sec. 4.1, we describe the experimental datasets and evaluation protocols. The implementation details of our model

are illustrated in Sec. 4.2. In Sec. 4.3, we compare the TacoDepth with previous Radar-Camera depth estimation approaches to demonstrate our state-of-the-art performance. The inference speed and model efficiency of different methods are evaluated and discussed in Sec. 4.4. In Sec. 4.5, we perform ablation studies to expound on our specific designs.

4.1. Datasets and Evaluation Protocols

Due to the scarcity of public datasets for Radar-Camera depth estimation, prior works [21, 27, 29, 30, 32, 38, 39, 41] only conduct experiments on nuScenes dataset [4] with 3D Radar. Recently, RadarCam-Depth [22] releases their ZJU-4DRadarCam dataset [22] with 4D Radar to alleviate this problem. We adopt these two datasets [4, 22] for experiments, proving our effectiveness on both 3D and 4D Radar.

NuScenes Dataset. As an outdoor driving dataset, the nuScenes [4] is collected by vehicles equipped with cameras, 3D Radar, LiDAR, and IMU. It contains 1,000 scenes and around 40,000 synchronized Radar-Camera keyframes captured in Boston and Singapore. We follow the same train-test split as prior arts [22, 27, 30, 32, 38, 41], with 700 scenes for training, 150 for validation, and 150 for testing.

ZJU-4DRadarCam Dataset. The dataset [22] is collected by a ground robot fitted with more advanced camera, 4D Radar, and LiDAR sensors, offering denser Radar data and LiDAR depth than the nuScenes [4] dataset. It comprises 33,409 Radar-Camera keyframes in total. We follow the official data split [22] with 29,312 frames for training and validation, and 4,097 samples for testing in our experiments.

Evaluation Protocols. We evaluate independent and plug-in models separately for fair comparisons on the two datasets [4, 22] with depth ranges of 50, 70, and 80 meters [22, 32, 38, 41]. On nuScenes [4], previous state-of-the-art methods [13, 21, 22, 27, 29, 32, 38, 41] are compared comprehensively to the best of our knowledge. For the recently published ZJU-4DRadarCam [22], since most prior works do not include experiments on the dataset, we can only follow the same comparative methods [22, 29, 38] and results as RadarCam-Depth [22]. Besides, we also evaluate plug-in models with different depth predictors [3, 36, 52] to showcase model flexibility on the ZJU-4DRadarCam [22].

Evaluation Metrics. We adopt the commonly-applied depth metrics MAE, RMSE, iMAE, iRMSE, δ_1 , and *Rel* as prior arts [22, 27, 32, 38]. See supplement for more details.

4.2. Implementation Details

Data Processing. We adhere to the data processing procedures of prior arts [22, 38]. For the nuScenes [4], the D_{acc} in Eq. 5 is generated by accumulating the D_{gt} of 160 nearby frames [22, 38]. For the ZJU-4DRadarCam dataset [22], the D_{acc} is obtained via the linear interpolation [1, 22] of D_{gt} .

Model Architecture. In line with prior arts [22, 38], the ResNet-18 [15] is adopted as the image encoder. The graph-

Type	Method	Radar Frames	Images	Time(ms)↓	0 - 50m		0 - 70m		0 - 80m	
					MAE↓	RMSE↓	MAE↓	RMSE↓	MAE↓	RMSE↓
Independent	Lin <i>et al.</i> [27] (IROS'20)	3	1	117.6	2034.9	4316.5	2294.7	5338.2	2371.0	5623.0
	RC-PDA [32] (CVPR'21)	5	3	79.2	2225.0	4156.5	3326.1	6700.6	3713.6	7692.8
	R4Dyn [13] (3DV'21)	4	1	—	—	—	—	—	—	6434.0
	DORN [29] (ICIP'21)	5(×3)	1	392.5	1926.6	4124.8	2380.6	5252.7	2467.7	5554.3
	Singh <i>et al.</i> [38] (CVPR'23)	1	1	94.2	1727.7	3746.8	2073.2	4590.7	2179.3	4898.7
	CaFNet [41] (IROS'24)	1	1	103.9	1674.2	3674.5	2010.3	4493.1	2109.8	4765.6
	Li <i>et al.</i> [21] (ECCV'24)	1	1	<u>67.6</u>	<u>1524.5</u>	<u>3567.3</u>	<u>1822.9</u>	<u>4303.6</u>	<u>1927.0</u>	<u>4609.6</u>
	TacoDepth (Ours)	1	1	26.7	1423.6	3275.8	1712.6	3960.5	1833.4	4150.2
Plug-in	RadarCam-Depth [22] (ICRA'24)	1	1	<u>358.3</u>	<u>1286.1</u>	<u>2964.3</u>	<u>1587.9</u>	<u>3662.5</u>	<u>1689.7</u>	<u>3948.0</u>
	TacoDepth (Ours)	1	1	29.3	1046.8	2487.5	1347.1	3152.8	1492.4	3324.8

Table 1. **Comparisons with state-of-the-art methods on the nuScenes dataset [4] (in millimeters).** Independent [13, 21, 27, 29, 32, 38, 41] and plug-in [22] models are evaluated separately, with maximum evaluation distances of 50, 70, and 80 meters as prior arts [22, 38]. Plug-in models are compared using the same depth predictor DPT-Hybrid [36] as RadarCam-Depth [22]. We report the average runtime of processing one 900×1600 frame and 30 Radar points by different methods on one NVIDIA RTX A6000 GPU. The inference time of plug-in models does not contain initial depth prediction. Some methods [13, 27, 29, 32] require multiple frames and Radar scans for inference, while others [21, 22, 38, 41] only need a single frame as input. The best performance is in boldface. Second best is underlined.

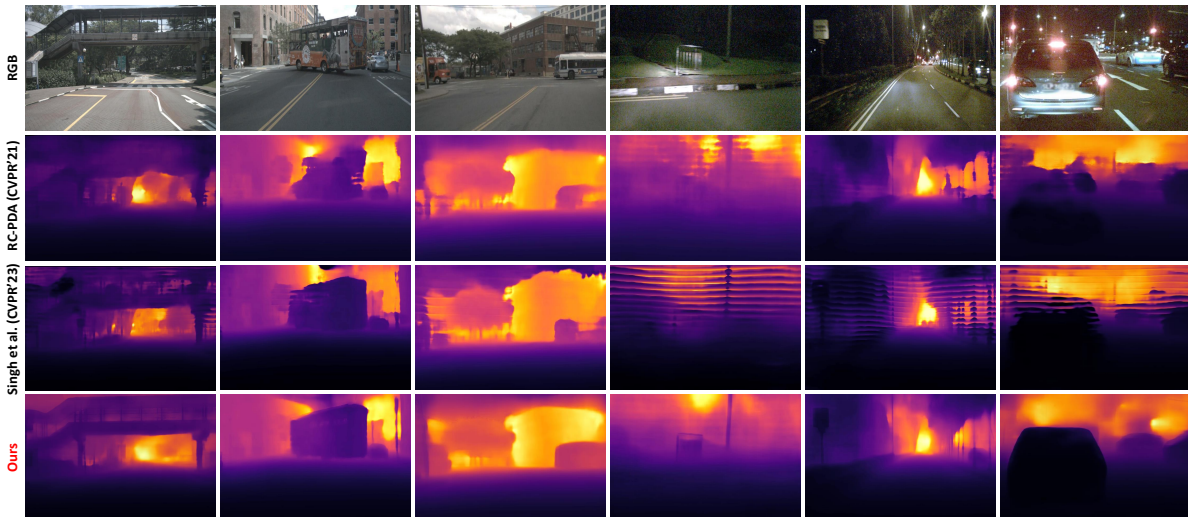


Figure 4. **Visual results of independent models on nuScenes [4].** Both daytime and nighttime samples are presented. Prior arts [32, 38] exhibit disrupted structures and noticeable artifacts. TacoDepth produces accurate depth with finer details and more complete structures.

based Radar structure extractor contains $L = 3$ layers with the GNN [12, 37] architecture. The widths a_l of Radar-centered areas in Eq. 1 and Eq. 2 are set to $\{48, 32, 16\}$ for the three layers. Refer to the supplement for more details.

Training Recipe. The model is trained by Adam optimizer on two NVIDIA A6000 GPUs with a batch size of 12 for 50 epochs. The initial learning rate is $1e^{-4}$ and decreases by $1e^{-5}$ for every ten epochs. The input image size is 900×1600 [22, 38] and 300×1280 [22] on nuScenes [4] and ZJU-4DRadarCam [22], respectively. The λ in Eq. 5 is set to one. All other settings are consistent with prior works [22, 38].

4.3. Comparisons with State-of-the-art Methods

Comparisons with Independent Models. Independent models [13, 21, 27, 29, 30, 32, 38, 39, 41] predict dense

metric depth without using relative depth predictors [3, 35, 36, 52]. Most of them adopt two-stage methods with intermediate quasi-dense depth, which are inefficient and not robust. Our TacoDepth significantly surpasses these methods in efficiency and accuracy with one-stage fusion. For example, in Table 1, compared with the recent CaFNet [41], our model reduces RMSE, MAE, and inference time by over 10.9%, 13.1%, and 74.3% on nuScenes dataset [4]. Additionally, Li *et al.* [21] aim to improve the training paradigm under sparse supervision by their Disruption-Compensation framework. Without using such advanced training and supervision strategy, TacoDepth still outperforms Li *et al.* [21] by over 60.5%, 4.9%, and 8.1% for runtime, MAE, and RMSE, showing the efficacy of our proposed architectures.

Similarly, in Table 2, compared with Singh *et al.* [38],

Type	Method	0 - 50m				0 - 70m				0 - 80m			
		MAE↓	RMSE↓	iMAE↓	iRMSE↓	MAE↓	RMSE↓	iMAE↓	iRMSE↓	MAE↓	RMSE↓	iMAE↓	iRMSE↓
Independent	DORN [29] (ICIP'21)	2210.2	4129.7	19.8	<u>31.9</u>	2402.2	4625.2	19.8	<u>31.9</u>	2447.6	4760.0	19.9	<u>31.9</u>
	Singh <i>et al.</i> [38] (CVPR'23)	<u>1785.4</u>	<u>3704.6</u>	<u>18.1</u>	35.3	<u>1932.7</u>	<u>4137.1</u>	<u>18.0</u>	35.2	<u>1979.5</u>	<u>4309.3</u>	<u>17.9</u>	35.1
	TacoDepth (Ours)	1120.1	2686.7	12.8	25.0	1181.8	2906.3	12.7	24.9	1201.1	2990.7	12.7	24.9
Plug-in	RadarCam-Depth [22] (ICRA'24)	<u>1067.5</u>	<u>2817.4</u>	<u>10.5</u>	<u>22.9</u>	<u>1157.0</u>	<u>3117.7</u>	<u>10.4</u>	<u>22.9</u>	<u>1183.5</u>	<u>3229.0</u>	<u>10.4</u>	<u>22.8</u>
	TacoDepth (Ours)	930.2	2477.3	9.3	20.8	983.1	2779.6	9.3	20.9	1032.5	2850.3	9.4	20.9

Table 2. **Comparisons with state-of-the-art methods on ZJU-4DRadarCam [22] (in millimeters).** Plug-in models are compared using the same relative depth predictor DPT-Hybrid [36]. Since many prior works do not include experiments on this new dataset, we adhere to the same compared methods [22, 29, 38] and metrics as RadarCam-Depth [22]. Best performance is in boldface. Second best is underlined.



Figure 5. **Visual results of plug-in models [22] on the ZJU-4DRadarCam [22].** The same depth predictor DPT-Hybrid [36] is adopted for fair comparisons. Regions with obvious differences are highlighted in the rectangular boxes. Best view zoomed in on-screen for details.

TacoDepth reduces depth errors by over 37.3%, 27.5%, 28.7%, and 29.1% for MAE, RMSE, iMAE, and iRMSE on ZJU-4DRadarCam [22]. The superior efficiency and accuracy prove the effectiveness of our one-stage model design.

Comparisons with Plug-in Models. Plug-in models [22] convert relative depth to metric depth by fusing the RGB and Radar data. Our method supports both independent and plug-in processing by the auxiliary input branch. For the plug-in mode, in Table 1, TacoDepth decreases the MAE and RMSE by over 11.7% and 13.9% than RadarCam-Depth [22] on nuScenes [4]. Owing to their complex four-stage framework [22], we even improve the speed by 91.8%. Similarly, in Table 2, TacoDepth reduces the MAE, RMSE, iMAE, and iRMSE by over 12.8%, 10.8%, 9.6%, and 8.3% on ZJU-4DRadarCam [22]. The results prove the generality and flexibility of TacoDepth, providing a better balance of model efficiency and accuracy for different users.

To be mentioned, in the plug-in mode, TacoDepth can

be compatible with various relative depth predictors [3, 36, 52]. It can benefit from stronger depth models [3, 52] to achieve higher accuracy, which will be presented in Table 4.

Qualitative Comparisons. The visual results of independent models [32, 38] are showcased in Fig. 4. Both daytime and nighttime samples are compared. TacoDepth can predict accurate depth maps with more complete structures (*e.g.*, the cars and buses) and more meticulous details (*e.g.*, the pedestrian overpass and metal guardrail). The plug-in models [22] are compared in Fig. 5. Based on the same depth predictor DPT-Hybrid [36], our method produces noticeably better structures and details in the rectangular boxes. The improvements are attributed to our graph-based Radar structure extractor and pyramid-based Radar fusion module, which extract and fuse Radar structures effectively.

Model Robustness. Multi-stage methods [27, 29, 32, 38, 41] predict quasi-dense depth as an intermediate step. However, as shown in Fig. 2, the intermediate results are still

Type	Method	Params (M) \downarrow	FLOPs (G) \downarrow	Time (ms) \downarrow
Independent	DORN [29] (ICIP'21)	183.38	923.47	392.5
	Singh <i>et al.</i> [38] (CVPR'23)	22.81	502.09	94.2
	TacoDepth (Ours)	13.47	139.30	26.7
Plug-in	RadarCam-Depth [22] (ICRA'24)	33.26	619.02	358.3
	TacoDepth (Ours)	14.25	139.87	29.3

Table 3. **Model efficiency.** We report FLOPs, model parameters, and runtime of different methods. Since varied depth predictors can be applied, the results of plug-in models do not contain initial depth prediction. FLOPs and runtime are evaluated with one 900 \times 1600 image and 30 Radar points on one NVIDIA A6000 GPU.

	Initial			RadarCam-Depth [22]			TacoDepth (Ours)		
	$\delta_1 \uparrow$	Rel \downarrow	MAE \downarrow	$\delta_1 \uparrow$	Rel \downarrow	MAE \downarrow	$\delta_1 \uparrow$	Rel \downarrow	MAE \downarrow
DPT-Hybrid [36]	0.903	0.092	–	0.921	0.087	1157.0	0.932	0.076	983.1
MiDaS-v3.1 [3]	0.917	0.081	–	0.926	0.086	1177.2	0.944	0.071	852.4
Depth-Anything-v2 [52]	0.932	0.069	–	0.940	0.073	924.7	0.961	0.059	730.2

Table 4. **Plug-in models with varied depth predictors.** Our method outperforms RadarCam-Depth [22] with different depth predictors [3, 36, 52] on ZJU-4DRadarCam [22] (0-70 meters).

sparse and noisy, especially on challenging nighttime and glaring scenes, leading to disrupted structures, blurred details, and obvious artifacts in their final depth predictions, as presented in Fig. 4. In contrast, we propose the one-stage TacoDepth without the quasi-dense depth. By effectively integrating the complementary image details and Radar structures, our model produces robust depth for both daytime and nighttime scenarios in Fig. 4. See supplement for more quantitative and visual results on nighttime scenes.

4.4. Model Efficiency

We evaluate the processing time of different methods in Table 1. Compared with the second-best independent model of Li *et al.* [21] and the plug-in model RadarCam-Depth [22], TacoDepth improves inference speed by 60.5% and 91.8%.

To further showcase our efficiency, we report model parameters and FLOPs in Table 3. Compared with the two-stage Singh *et al.* [38], the one-stage TacoDepth reduces the parameters and FLOPs by 40.9% and 72.2%. Compared with the four-stage plug-in model RadarCam-Depth [22], we decrease parameters and FLOPs by 57.1% and 77.4%.

Note that, the differences between the plug-in and independent modes of our method arise from the auxiliary branch to fuse initial relative depth. TacoDepth achieves real-time processing of 37.5 fps by independent inference.

4.5. Ablation Studies

Plug-in Inference. In Table 4, our TacoDepth outperforms the RadarCam-Depth [22] with three different relative depth predictors [3, 36, 52]. Using more advanced depth predictors, *e.g.*, MiDaS-v3.1 [3] and Depth-Anything-v2 [52], can further boost our accuracy without extra effort. The results demonstrate the versatility and flexibility of our approach.

Efficacy of TacoDepth. In Table 5, we ablate the graph-

Method	RGB	Radar	GE	PF	MAE \downarrow	RMSE \downarrow
RGB Baseline	✓	✗	✗	✗	2474.3	5402.1
Singh <i>et al.</i> [38] (CVPR'23)	✓	✓	✗	✗	2073.2	4590.7
TacoDepth (<i>w/o</i> GE)	✓	✓	✗	✓	<u>1815.6</u>	<u>4189.8</u>
TacoDepth (Ours)	✓	✓	✓	✓	1712.6	3960.5

Table 5. **Efficacy of the TacoDepth.** We ablate the effectiveness of graph-based Radar structure extractor (GE) and pyramid-based Radar fusion (PF) for Radar structure extraction and integration. We adopt the same baseline as Singh *et al.* [38]. TacoDepth (*w/o* GE) uses the same MLP to extract Radar point features as prior art [38]. The results are evaluated on nuScenes [4] in 0-70 meters.

Metric	$L = 1$	$L = 2$	$L = 3$	$L = 4$
MAE \downarrow	1840.6	1787.8	1712.6	1729.3
RMSE \downarrow	4203.7	4046.9	3960.5	3984.2

Table 6. **Layer number L.** Results are on nuScenes [4] in 0-70m.

based Radar structure extractor (GE) and pyramid-based Radar fusion module (PF). With the same MLP to extract Radar point features [38], TacoDepth (*w/o* GE) reduces MAE and RMSE by 12.4% and 8.7% than Singh *et al.* [38], which are attributed to the PF. Replacing the MLP [38] with GE further decreases MAE and RMSE by 5.7% and 5.5%.

We adopt the RGB baseline of Singh *et al.* [38], a common single-image depth U-Net. Overall, TacoDepth improves accuracy beyond the baseline by 30.8% and 26.7% (MAE and RMSE), proving the efficacy of our approach.

Layer Number L. In Table 6, we ablate the layer number L of GE and PF. Compared with shallow layers ($L = 1, 2$), deeper layers ($L = 3$) better capture structures of point clouds [42, 46], producing higher accuracy. Due to Radar sparsity, more layers ($L = 4$) does not yield improvements but decreases efficiency. We adopt $L = 3$ in experiments.

5. Conclusion

In this paper, we propose TacoDepth, an efficient and accurate Radar-Camera depth estimation model with one-stage fusion. Different from the multi-stage methods with quasi-dense depth, TacoDepth utilizes the graph-based Radar structure extractor and pyramid-based Radar fusion module to capture and integrate Radar features, achieving superior efficiency and robustness. Moreover, TacoDepth is flexible for independent and plug-in processing, offering a better balance of speed and accuracy. Our work provides a new perspective on the efficient Radar-Camera depth estimation.

Limitations. We currently provide one efficient implementation of our TacoDepth. In future work, more techniques can be explored for varied performances and applications.

Acknowledgments. The study is supported under RIE2020 Industry Alignment Fund – Industry Collaboration Projects (IAF-ICP) Funding Initiative, as well as cash and in-kind contribution from the industry partner(s). This research is also supported by the MoE AcRF Tier 1 grant (RG14/22).

TacoDepth: Towards Efficient Radar-Camera Depth Estimation with One-stage Fusion

Supplementary Material

This supplement contains the following contents:

- More quantitative and qualitative results.
- More details on experimental settings.
- More implementation details for TacoDepth.

6. More Experimental Results

6.1. Quasi-dense Depth in Prior Arts

As mentioned in Fig. 2 and line 050 of our main paper, previous multi-stage approaches [22, 27, 30, 32, 38, 41] predict intermediate quasi-dense depth, which remains sparse and noisy. We provide more visual results of their intermediate and final depth in Fig. 6. Flawed quasi-dense results lead to blurred details, disrupted structures, and noticeable artifacts in their final predictions, especially on nighttime and glaring scenes, which limits the robustness of their models.

6.2. Model Robustness

We show more results to prove our robustness on both daytime and nighttime scenes (Sec. 4.3, line 469, main paper).

Quantitative Results. As shown in Table 7, on the nuScenes [4] dataset, we compare our model with the state-of-the-art two-stage method of Singh *et al.* [38] on daytime and nighttime scenes separately. For daytime samples, our method reduces MAE and RMSE by 12.9% and 11.0%. On nighttime scenarios, TacoDepth decreases MAE and RMSE by 29.1% and 25.2%. The results can further highlight our superior robustness under challenging nighttime conditions.

Visual Results. We present more visual comparisons for daytime (Fig. 10, Fig. 11) and nighttime samples (Fig. 12, Fig. 13). Without relying on the intermediate quasi-dense depth [22, 27, 29, 30, 32, 38, 39, 41], TacoDepth robustly predicts accurate depth with more complete structures and meticulous details on daytime and nighttime scenes.

Reasons for Robustness. Our robustness can be attributed to three factors. Firstly, our one-stage framework avoids reliance on intermediate results, thereby preventing the negative impacts of defective quasi-dense depth. Secondly, our graph-based Radar structure extractor captures the informative geometric structures and graph topologies. Compared with the simple point features [38], the overall structures are more robust and resilient [12, 37, 46] against Radar outliers. Furthermore, our pyramid-based Radar fusion module integrates Radar and image information from shallow to deep layers effectively. The Radar-centered flash attention can efficiently build cross-modal correspondences and suppress unreliable Radar points, which will be discussed in Sec. 6.3.

Scene	Method	0 - 50m		0 - 70m		0 - 80m	
		MAE↓	RMSE↓	MAE↓	RMSE↓	MAE↓	RMSE↓
Daytime	Singh <i>et al.</i> [38] (CVPR'23)	1618.9	3613.0	1924.7	4359.2	2017.9	4632.5
	TacoDepth (Ours)	1389.5	3227.3	1680.9	3897.1	1782.4	4092.3
Nighttime	Singh <i>et al.</i> [38] (CVPR'23)	2340.8	4683.8	2863.9	5935.4	3012.9	6338.3
	TacoDepth (Ours)	1673.6	3631.4	1944.8	4425.3	2207.6	4574.8
Overall	Singh <i>et al.</i> [38] (CVPR'23)	1727.7	3746.8	2073.2	4590.7	2179.3	4898.7
	TacoDepth (Ours)	1423.6	3275.8	1712.6	3960.5	1833.4	4150.2

Table 7. **Comparisons on daytime and nighttime scenarios of the nuScenes [4] dataset.** We calculate the average performance improvements across the three different depth ranges. On daytime scenes, compared with Singh *et al.* [38], our method reduces MAE and RMSE by 12.9% and 11.0%. On nighttime scenes, TacoDepth decreases MAE and RMSE by 29.1% and 25.2%. Overall, our model improves the performance by 17.0% and 13.9%. These results further prove our strong robustness on challenging scenarios.

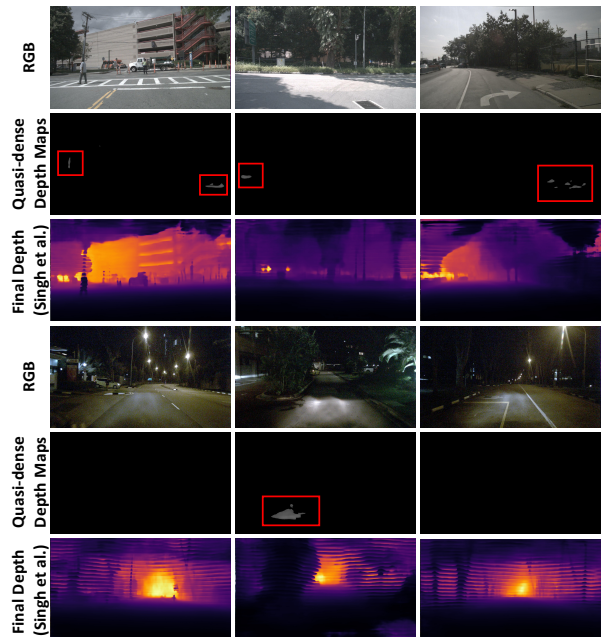


Figure 6. **Intermediate quasi-dense depth [22, 27, 29, 30, 32, 38, 39, 41] remains sparse and noisy.** We showcase more intermediate and final results from the previous two-stage method of Singh *et al.* [38] (CVPR'23). Pixels with valid depth values in the quasi-dense depth are visualized by gray areas in red rectangular boxes. Only few pixels exhibit valid depth. For some nighttime and glaring conditions, even no pixels are predicted with depth values. Due to the multi-stage frameworks [22, 27, 29, 30, 32, 38, 39, 41], the defective intermediate depth could lead to blurred details, disrupted structures, and noticeable artifacts in their final predictions. Our TacoDepth does not rely on quasi-dense depth, achieving superior efficiency, accuracy, and robustness with one-stage fusion.



Figure 7. **Visualization of attention maps.** Some accurate Radar points are projected onto the image plane, as indicated by the colored points and indices. For each Radar point, the attention computation is confined to Radar-centered areas to maintain efficiency. In the attention maps, brighter colors represent higher attention scores. Our Radar-centered flash attention can effectively focus on correct corresponding regions and establish cross-modal correspondences. The attention maps also accurately distinguish between foreground and background, *e.g.*, **shrub**, **road surface**, **car body**, **side mirror**, **stone tablet**, **car rear**, and **billboard**. Best view zoomed in on-screen for details.

Module	MAE↓	RMSE↓	FLOPs (G)↓
Attention [43]	1982.4	4428.3	835.4
Radar-centered flash attention	1712.6	3960.5	139.3

Table 8. **Ablation on the Radar-centered flash attention.** We compare the original attention [43] with our Radar-centered flash attention implemented in TacoDepth. The MAE and RMSE are evaluated on the nuScenes dataset [4] in 0-70 meters. The FLOPs are reported for the whole model to process one 900×1600 image and 30 Radar points. Without restricting the Radar-centered areas, the original attention [43] fuses irrelevant image pixels and Radar points, resulting in unacceptable computational overheads. In contrast, our Radar-centered flash attention can effectively establish the cross-modal correspondences and maintain model efficiency.

Metric	$a_l = \{32, 16, 8\}$	$a_l = \{48, 32, 16\}$	$a_l = \{64, 48, 32\}$
MAE↓	1811.3	1712.6	1785.7
RMSE↓	4179.8	3960.5	4082.2

Table 9. **Ablation on the widths a_l of Radar-centered areas.** The results are evaluated on the nuScenes dataset [4] in 0-70 meters. Reducing a_l could exclude some valid Radar points and image pixels from the fusion process, leading to a decrease in depth accuracy. On the other hand, since the horizontal Radar coordinates are relatively precise, using larger a_l could incorporate some irrelevant points and increase computational costs. Thus, we adopt $a_l = \{48, 32, 16\}$ in our experiments for the three fusion layers.

6.3. Radar-centered Flash Attention

In Sec. 3.2, line 252 of the main paper, we propose the Radar-centered flash attention mechanism in our pyramid-based Radar fusion module to build cross-modal correspondences between Radar points and RGB pixels. Here, we provide additional experiments to demonstrate its efficacy.

Visualization of Attention Maps. In Fig. 7, we visualize our Radar-centered flash attention. Several accurate Radar points are projected onto the image plane. The attention is calculated within Radar-centered areas for efficiency. External pixels and points could not be correlated, since horizontal Radar coordinates are relatively precise. As depicted in Fig. 7, our Radar-centered flash attention can effectively focus on the correct corresponding regions and establish cross-modal correspondences. The attention maps also accurately distinguish between foreground and background.

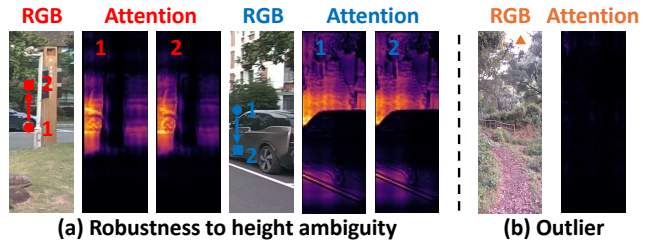


Figure 8. **(a) Robustness to height ambiguity of 3D Radar.** The 3D Radar suffers from height ambiguity [32] due to insufficient antenna elements along the elevation axis. We simulate this issue by manually altering the vertical coordinates of some accurate Radar points (represented by the circles). Even with perturbed Radar inputs (represented by the squares), our attention maps can still identify the correct corresponding regions in the images, *e.g.*, **the car wheel** and **the trees**. **(b) Robustness to Radar outliers.** For Radar outliers with inaccurate point coordinates or depth values, *e.g.*, **the orange triangle in the sky**, TacoDepth suppresses these noisy points with low attention scores, such as the black attention map. Image pixels are only integrated with reliable Radar points.

Robustness to Height Ambiguity. Due to insufficient antenna elements along the elevation axis, 3D Radar suffers from height ambiguity [4, 32, 38] with unreliable vertical coordinates. We simulate this issue by manually altering the height dimensions of some accurate Radar points. As shown in Fig. 8(a), even with perturbed Radar inputs, our attention maps still identify correct corresponding regions.

Robustness to Radar Outliers. The accuracy of Radar is generally lower than LiDAR. When faced with Radar outliers, as shown in Fig. 8(b), our Radar-centered flash attention can suppress the noisy points with low attention scores. Image pixels will only be integrated with reliable Radar points, which can further enhance the model robustness.

Ablation on Radar-centered Flash Attention. Following Sec. 4.5, line 510 of our paper, we conduct an ablation on the Radar-centered flash attention. In Table 8, we compare the original attention [43] with our Radar-centered flash attention implemented in TacoDepth. Without restricting the Radar-centered areas, the original attention [43] fuses irrelevant image pixels and Radar points with heavy computa-

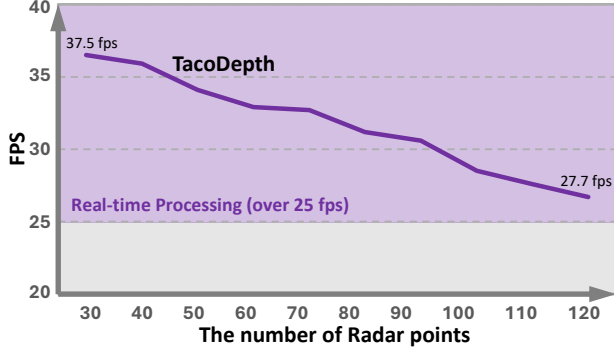


Figure 9. **Inference speed and Radar point numbers.** We evaluate the Frames Per Second (FPS) of our TacoDepth with different amounts of input Radar points. For the nuScenes dataset [4], the average and maximum numbers of Radar points per sample are 96.84 and 125. Our model achieves real-time processing (e.g., over 27.7 fps) across typical Radar point numbers on nuScenes [4].

tional overheads. In contrast, our Radar-centered flash attention reduces the MAE, RMSE, and FLOPs by 13.6%, 10.6%, and 83.3%, which effectively establishes the cross-modal correspondences and maintains model efficiency.

Ablation on the widths a_l of Radar-centered areas. As noted in Sec. 4.2, line 399 of the main paper, we set $a_l = \{48, 32, 16\}$. Here, in Table 9, we ablate this specific choice. Reducing a_l could exclude some valid Radar points and image pixels from the fusion process, leading to a decrease in depth accuracy. On the other hand, since the horizontal Radar coordinates are relatively precise, using larger a_l could incorporate some irrelevant points and increase computational costs. Therefore, we adopt $a_l = \{48, 32, 16\}$ in all other experiments for the three fusion layers.

6.4. Model Efficiency

In Table 1 and Table 3 of the main manuscript, we compare the model efficiency under one 900×1600 image and 30 Radar points. Here, in Fig. 9, we further evaluate the inference speed of our TacoDepth with varying numbers of Radar points as input. From 30 to 120 Radar points, our model achieves real-time processing across the typical range of Radar point numbers on the nuScenes [4] dataset.

Multi-stage methods [22, 27, 29, 38, 41] are complex and inefficient. Two-stage independent models [27, 29, 30, 32, 38, 39, 41] use two separate networks for intermediate and final depth. The four-stage plug-in RadarCam-Depth [22] employs least-squares optimization or RANSAC [11] for global alignment. TacoDepth noticeably outperforms these models in efficiency with one-stage fusion.

6.5. More Qualitative Results

We show more visual comparisons in Fig. 10, 11, 12, and 13. The Fig. 10 and Fig. 11 contain daytime samples, while Fig. 12 and Fig. 13 present nighttime scenarios.

7. More Details on Experimental Settings

7.1. Depth Metrics

As described in Sec. 4.1 of the main paper, following prior arts [22, 27, 32, 38], we adopt the commonly-applied depth metrics MAE, RMSE, iMAE, iRMSE, δ_1 , and Rel for comparisons. Their definitions are specified in this section.

For Radar-Camera depth estimation, most previous works [22, 27, 29, 30, 32, 38, 41] utilize MAE and RMSE for evaluations. Besides, we also follow RadarCam-Depth [22] to report iMAE and iRMSE on ZJU-4DRadarCam [22]. The iMAE and iRMSE measure errors of inverse depth (i.e., disparity), which are less sensitive to varied depth ranges (50, 70, or 80 meters).

To compare the plug-in models [22] with different depth predictors [3, 35, 36, 52] (Table 4, main paper), we adopt the δ_1 and Rel . These metrics are formulated as follows:

- Mean Absolute Error (MAE):

$$\frac{1}{|\Omega_{gt}|} \sum_{\Omega_{gt}} |D - D_{gt}|;$$

- Root Mean Square Error (RMSE):

$$\left(\frac{1}{|\Omega_{gt}|} \sum_{\Omega_{gt}} |D - D_{gt}|^2 \right)^{\frac{1}{2}};$$

- Inverse Mean Absolute Error (iMAE):

$$\frac{1}{|\Omega_{gt}|} \sum_{\Omega_{gt}} \left| \frac{1}{D} - \frac{1}{D_{gt}} \right|;$$

- Inverse Root Mean Square Error (iRMSE):

$$\left(\frac{1}{|\Omega_{gt}|} \sum_{\Omega_{gt}} \left| \frac{1}{D} - \frac{1}{D_{gt}} \right|^2 \right)^{\frac{1}{2}};$$

- Mean Relative Error (Rel):

$$\frac{1}{|\Omega_{gt}|} \sum_{\Omega_{gt}} \frac{|D - D_{gt}|}{D_{gt}};$$

- δ_1 Threshold: pixel percentage of prediction D such that $\max(\frac{D}{D_{gt}}, \frac{D_{gt}}{D}) = \delta < 1.25$, where D denotes the predicted depth. D_{gt} represents the depth ground truth. Ω_{gt} depicts the mask of D_{gt} with valid depth values.

7.2. Data Processing

We further illustrate the data processing procedures for the nuScenes [4] and ZJU-4DRadarCam [22] datasets (Sec. 4.2, line 390, main paper). Following prior arts [22, 27, 29, 32, 38], on the nuScenes [4] dataset, we accumulate 80 future and 80 past LiDAR frames to generate D_{acc} . Dynamic objects annotated by bounding boxes are removed before the projection. On ZJU-4DRadarCam [22], since it contains denser LiDAR returns and depth maps, we directly interpolate D_{gt} to obtain D_{acc} as the RadarCam-Depth [22].

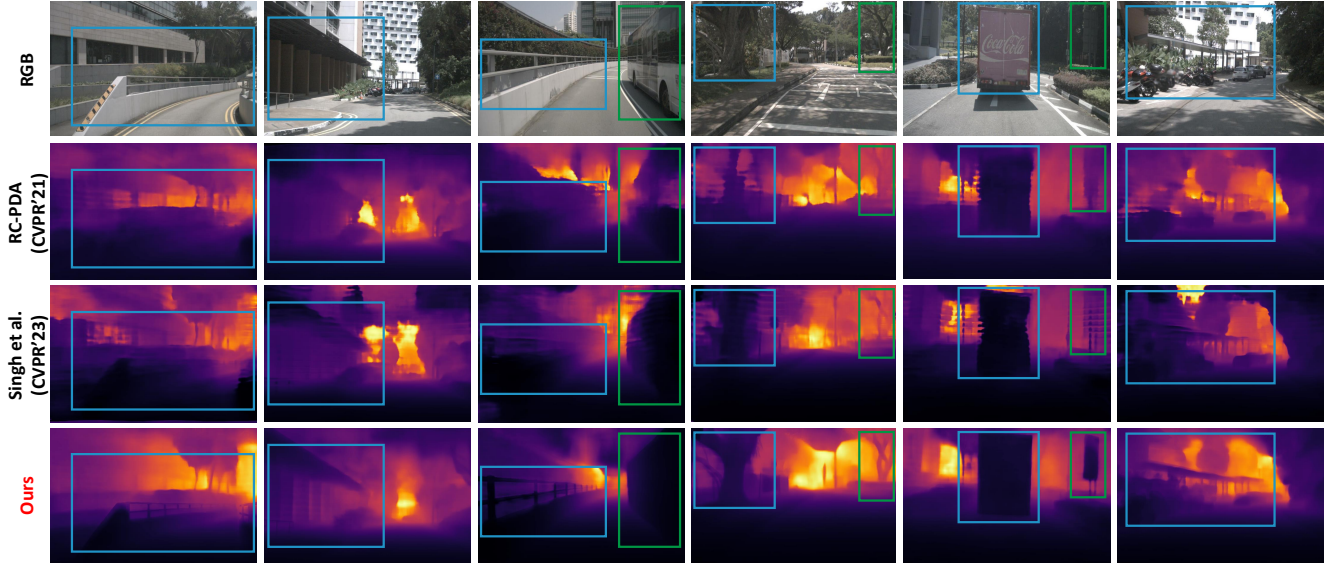


Figure 10. **Visual results on daytime scenes.** Previous multi-stage methods [32, 38] exhibit disrupted structures, blurred details, or noticeable artifacts. Our TacoDepth can predict accurate depth with complete structures and fine details. Best view zoomed in on-screen.

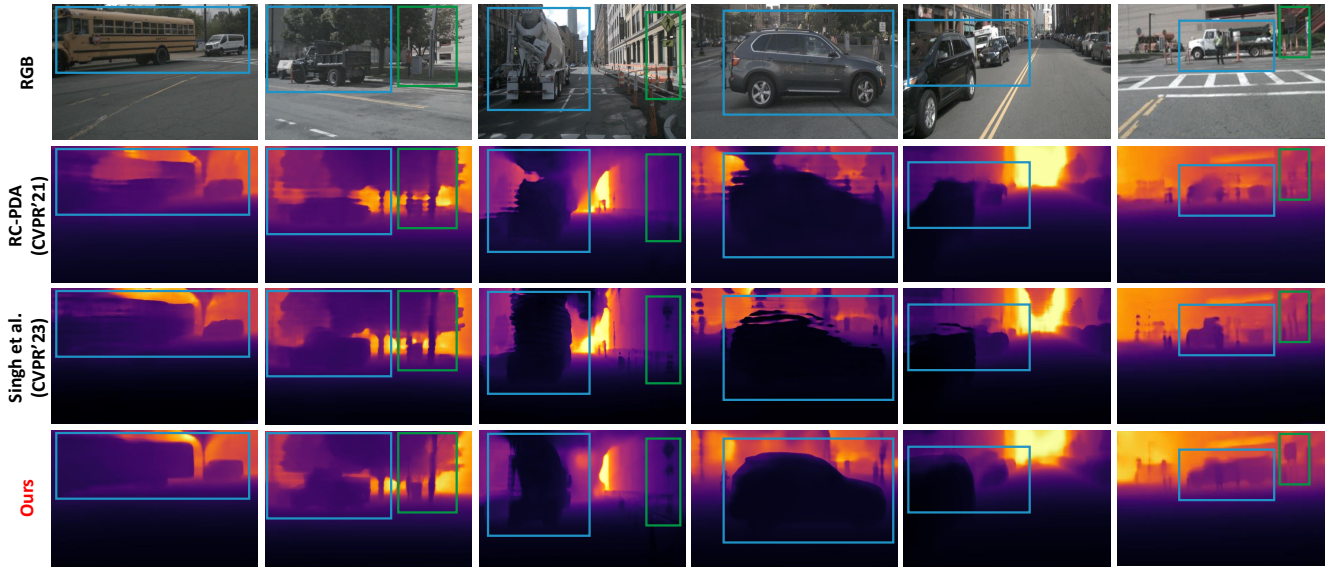


Figure 11. **Visual results on daytime scenes.** Previous multi-stage methods [32, 38] exhibit disrupted structures, blurred details, or noticeable artifacts. Our TacoDepth can predict accurate depth with complete structures and fine details. Best view zoomed in on-screen.

8. More Implementation Details for TacoDepth

Following Sec. 4.2, line 400 of the main paper, we present more detailed descriptions regarding our implementations.

8.1. Graph-based Radar Structure Extractor

As mentioned in Sec. 3.1, line 190 of the paper, our graph-based Radar structure extractor captures the geometric structures of Radar point clouds, involving a lightweight GNN [12, 37, 46] architecture with $L = 3$ layers. Each

layer comprises a node and an edge generator. For one Radar point, the node generator extracts local node features from K -nearest neighboring points using MLPs, maxpooling, and concatenation. With the node features, the edge generator builds a soft adjacency matrix of Radar points as the edge feature via MLPs and attention [12, 43]. Node features can then be aggregated along edges by PCA-GM [45]. Thus, from shallow to deep layers, graph-based Radar structure extractor captures detailed coordinates and overall topologies, which are more robust to outliers [12, 37, 46].



Figure 12. **Visual results on nighttime scenes.** Previous multi-stage methods [32, 38] rely on the intermediate quasi-dense results, which lack robustness, producing final depth with disrupted structures or even obvious artifacts on nighttime scenes. In contrast, our TacoDepth predicts more accurate depth with complete structures and fine details, showcasing our superior robustness. Best view zoomed in on-screen.

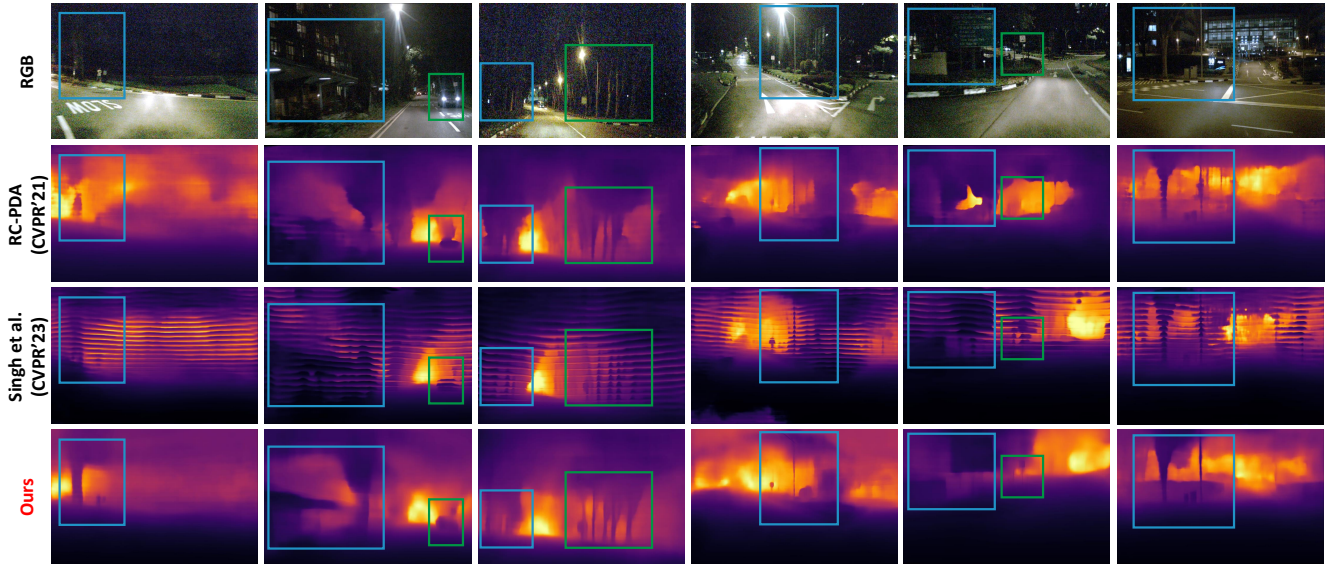


Figure 13. **Visual results on nighttime scenes.** Previous multi-stage methods [32, 38] rely on the intermediate quasi-dense results, which lack robustness, producing final depth with disrupted structures or even obvious artifacts on nighttime scenes. In contrast, our TacoDepth predicts more accurate depth with complete structures and fine details, showcasing our superior robustness. Best view zoomed in on-screen.

8.2. Depth Decoder

With the fused features, a common decoder [3, 22, 32, 35, 38] is employed to produce depth results (line 220, main paper). Specifically, resolutions are gradually increased while channel numbers are decreased. Skip connections are adopted to restore depth details. At last, an adaptive output module [35] adjusts the channel and restores depth maps.

8.3. Auxiliary Input Branch

TacoDepth is flexible for independent and plug-in inference (Sec. 3.3, main paper). For the plug-in mode, an auxiliary branch processes initial relative depth [3, 36, 52]. To be specific, convolution extracts features from initial depth, which are then fused with RGB features by concatenation and convolution. Other steps are identical to the independent mode.

8.4. The Name of TacoDepth

Ultimately, we would like to explain the naming of our proposed framework. We name it TacoDepth for two reasons. Firstly, TacoDepth is an acronym derived from the words in the title of our paper, representing our key objectives and focus, such as efficient, Radar, camera, depth, and one-stage. Moreover, our task shares similarities with the concept of a taco. Just as a taco wraps and blends diverse ingredients to create a new flavor, our framework aims to fuse the information from multiple sensors and modalities, yielding a more accurate, effective, and robust depth estimation model.

References

- [1] C Bradford Barber, David P Dobkin, and Hannu Huhdanpaa. The quickhull algorithm for convex hulls. *ACM Transactions on Mathematical Software (TOMS)*, 22(4):469–483, 1996. 5
- [2] Oded Bialer and Yuval Haitman. Radsimreal: Bridging the gap between synthetic and real data in radar object detection with simulation. In *Proceedings of the IEEE/CVF Conference on Computer Vision and Pattern Recognition (CVPR)*, pages 15407–15416, 2024. 1, 2
- [3] Reiner Birkel, Diana Wofk, and Matthias Müller. Midas v3. 1—a model zoo for robust monocular relative depth estimation. *arXiv preprint arXiv:2307.14460*, 2023. 1, 2, 4, 5, 6, 7, 8, 3
- [4] Holger Caesar, Varun Bankiti, Alex H. Lang, Sourabh Vora, Venice Erin Liong, Qiang Xu, Anush Krishnan, Yu Pan, Giancarlo Baldan, and Oscar Beijbom. nuscenes: A multi-modal dataset for autonomous driving. In *Proceedings of the IEEE/CVF Conference on Computer Vision and Pattern Recognition (CVPR)*, pages 11618–11628, 2020. 1, 2, 5, 6, 7, 8, 3
- [5] Yujeong Chae, Hyeonseong Kim, and Kuk-Jin Yoon. Towards robust 3d object detection with lidar and 4d radar fusion in various weather conditions. In *Proceedings of the IEEE/CVF Conference on Computer Vision and Pattern Recognition (CVPR)*, pages 15162–15172, 2024. 1, 2
- [6] Feipeng Chen, Lihui Wang, Pinzhang Zhao, and Jian Wei. 3d grid-based vdbscan clustering and radar-monocular depth completion. *IEEE Sensors Journal*, 2024. 1
- [7] Tri Dao. Flashattention-2: Faster attention with better parallelism and work partitioning. *arXiv preprint arXiv:2307.08691*, 2023. 4
- [8] Tri Dao, Dan Fu, Stefano Ermon, Atri Rudra, and Christopher Ré. Flashattention: Fast and memory-efficient exact attention with io-awareness. 35, 2022. 2, 4
- [9] Fangqiang Ding, Andras Palffy, Dariu M. Gavrilă, and Chris Xiaoxuan Lu. Hidden gems: 4d radar scene flow learning using cross-modal supervision. In *Proceedings of the IEEE/CVF Conference on Computer Vision and Pattern Recognition (CVPR)*, pages 9340–9349, 2023. 1, 2
- [10] Haoqi Fan, Bo Xiong, Karttikeya Mangalam, Yanghao Li, Zhicheng Yan, Jitendra Malik, and Christoph Feichtenhofer. Multiscale vision transformers. In *Proceedings of the IEEE/CVF International Conference on Computer Vision (ICCV)*, pages 6824–6835, 2021. 2, 4
- [11] Martin A Fischler and Robert C Bolles. Random sample consensus: a paradigm for model fitting with applications to image analysis and automated cartography. *Communications of the ACM*, 24(6):381–395, 1981. 3
- [12] Kexue Fu, Shaolei Liu, Xiaoyuan Luo, and Manning Wang. Robust point cloud registration framework based on deep graph matching. In *Proceedings of the IEEE/CVF Conference on Computer Vision and Pattern Recognition (CVPR)*, pages 8893–8902, 2021. 2, 3, 4, 6, 1
- [13] Stefano Gasperini, Patrick Koch, Vinzenz Dallabetta, Nassir Navab, Benjamin Busam, and Federico Tombari. R4dyn: Exploring radar for self-supervised monocular depth estimation of dynamic scenes. In *International Conference on 3D Vision (3DV)*, pages 751–760, 2021. 1, 5, 6
- [14] Kyle Harlow, Hyesu Jang, Timothy D. Barfoot, Ayoung Kim, and Christoffer Heckman. A new wave in robotics: Survey on recent mmwave radar applications in robotics. *IEEE Transactions on Robotics*, 40:4544–4560, 2024. 1, 2
- [15] Kaiming He, Xiangyu Zhang, Shaoqing Ren, and Jian Sun. Deep residual learning for image recognition. In *Proceedings of the IEEE/CVF Conference on Computer Vision and Pattern Recognition (CVPR)*, pages 770–778, 2016. 2, 4, 5
- [16] Daniel Casado Herraiz, Matthias Zeller, Le Chang, Ignacio Vizzo, Michael Heidingsfeld, and Cyrill Stachniss. Radar-only odometry and mapping for autonomous vehicles. In *2024 IEEE International Conference on Robotics and Automation (ICRA)*, pages 539–548. IEEE, 2019. 1, 2
- [17] Tianshu Huang, John Miller, Akarsh Prabhakara, Tao Jin, Tarana Laroia, Zico Kolter, and Anthony Rowe. Dart: Implicit doppler tomography for radar novel view synthesis. In *Proceedings of the IEEE/CVF Conference on Computer Vision and Pattern Recognition (CVPR)*, pages 24118–24129, 2024. 1, 2
- [18] Andrey Ignatov, Grigory Malivenko, David Plowman, Samarth Shukla, and Radu Timofte. Fast and accurate single-image depth estimation on mobile devices, mobile ai 2021 challenge: Report. In *Proceedings of the IEEE/CVF Conference on Computer Vision and Pattern Recognition (CVPR) Workshops*, pages 2545–2557, 2021. 2
- [19] Yinuo Jiang, Beitong Zhou, Xiaoyu Liu, Qingyi Li, and Cheng Cheng. Gtinet: Global topology-aware interactions for unsupervised point cloud registration. *IEEE Transactions on Circuits and Systems for Video Technology*, 34(7): 6363–6375, 2024. 2
- [20] Alex Krizhevsky, Ilya Sutskever, and Geoffrey E Hinton. Imagenet classification with deep convolutional neural networks. In *Advances in neural information processing systems*, 2012. 2, 4
- [21] Huadong Li, Minhao Jing, Jiajun Liang, Haoqiang Fan, and Renhe Ji. Sparse beats dense: Rethinking supervision in radar-camera depth completion. *arXiv preprint arXiv:2312.00844*, 2023. 1, 5, 6, 8
- [22] Han Li, Yukai Ma, Yaqing Gu, Kewei Hu, Yong Liu, and Xingxing Zuo. Radarcam-depth: Radar-camera fusion for depth estimation with learned metric scale. *arXiv preprint arXiv: 2401.04325*, 2024. 1, 2, 3, 4, 5, 6, 7, 8
- [23] Jiaqi Li, Yiran Wang, Zihao Huang, Jinghong Zheng, Ke Xian, Zhiguo Cao, and Jianming Zhang. Diffusion-

- augmented depth prediction with sparse annotations. In *Proceedings of the 31st ACM International Conference on Multimedia*, page 2865–2876, New York, NY, USA, 2023. Association for Computing Machinery. 1
- [24] Jiaqi Li, Yiran Wang, Jinghong Zheng, Zihao Huang, Ke Xian, Zhiguo Cao, and Jianming Zhang. Self-distilled depth refinement with noisy poisson fusion, 2024. 2
- [25] Xingyi Li, Chaoyi Hong, Yiran Wang, Zhiguo Cao, Ke Xian, and Guosheng Lin. Symmnerf: Learning to explore symmetry prior for single-view view synthesis. In *Proceedings of the Asian Conference on Computer Vision (ACCV)*, pages 1726–1742, 2022. 2
- [26] Zecheng Li, Yuying Song, Fuyuan Ai, Chunyi Song, and Zhiwei Xu. Semantic-guided depth completion from monocular images and 4d radar data. *IEEE Transactions on Intelligent Vehicles*, pages 1–13, 2024. 1
- [27] Juan-Ting Lin, Dengxin Dai, and Luc Van Gool. Depth estimation from monocular images and sparse radar data. In *IEEE/RSJ International Conference on Intelligent Robots and Systems (IROS)*, pages 10233–10240. IEEE, 2020. 1, 2, 3, 4, 5, 6, 7
- [28] Zhiwei Lin, Zhe Liu, Zhongyu Xia, Xinhao Wang, Yongtao Wang, Shengxiang Qi, Yang Dong, Nan Dong, Le Zhang, and Ce Zhu. Rebevdet: Radar-camera fusion in bird’s eye view for 3d object detection. pages 14928–14937, 2024. 2
- [29] Chen-Chou Lo and Patrick Vandewalle. Depth estimation from monocular images and sparse radar using deep ordinal regression network. In *IEEE International Conference on Image Processing (ICIP)*, pages 3343–3347, 2021. 1, 2, 3, 4, 5, 6, 7, 8
- [30] Chen-Chou Lo and Patrick Vandewalle. Rcdpt: Radar-camera fusion dense prediction transformer. In *IEEE International Conference on Acoustics, Speech and Signal Processing (ICASSP)*, pages 1–5. IEEE, 2023. 1, 2, 3, 4, 5, 6
- [31] Chen-Chou Lo and Patrick Vandewalle. Expanding sparse radar depth based on joint bilateral filter for radar-guided monocular depth estimation. *Sensors*, 24(6):1864, 2024.
- [32] Yunfei Long, Daniel Morris, Xiaoming Liu, Marcos Castro, Punarjay Chakravarty, and Praveen Narayanan. Radar-camera pixel depth association for depth completion. In *Proceedings of the IEEE/CVF Conference on Computer Vision and Pattern Recognition (CVPR)*, pages 12507–12516, 2021. 1, 2, 3, 4, 5, 6, 7
- [33] Guohao Peng, Heshan Li, Yangyang Zhao, Jun Zhang, Zhenyu Wu, Pengyu Zheng, and Danwei Wang. Transloc4d: Transformer-based 4d radar place recognition. In *Proceedings of the IEEE/CVF Conference on Computer Vision and Pattern Recognition (CVPR)*, pages 17595–17605, 2024. 1, 2
- [34] Pierluigi Zama Ramirez, Fabio Tosi, Luigi Di Stefano, Radu Timofte, Alex Costanzino, Matteo Poggi, Samuele Salti, Stefano Mattoccia, Yangyang Zhang, Cailin Wu, Zhuangda He, Shuangshuang Yin, Jiayu Dong, Yangchenxu Liu, Hao Jiang, Jun Shi, Yong A, Yixiang Jin, Dingzhe Li, Bingxin Ke, Anton Obukhov, Tinafu Wang, Nando Metzger, Shengyu Huang, Konrad Schindler, Yachuan Huang, Jiaqi Li, Junrui Zhang, Yiran Wang, Zihao Huang, Tianqi Liu, Zhiguo Cao, Pengzhi Li, Jui-Lin Wang, Wenjie Zhu, Hui Geng, Yuxin Zhang, Long Lan, Kele Xu, Tao Sun, Qisheng Xu, Sourav Saini, Aashray Gupta, Sahaj K. Mistry, Aryan Shukla, Vinit Jakhetiya, Sunil Jaiswal, Yuejin Sun, Zhuofan Zheng, Yi Ning, Jen-Hao Cheng, Hou-I Liu, Hsiang-Wei Huang, Cheng-Yen Yang, Zhongyu Jiang, Yi-Hao Peng, Aishi Huang, and Jenq-Neng Hwang. Ntire 2024 challenge on hr depth from images of specular and transparent surfaces. In *Proceedings of the IEEE/CVF Conference on Computer Vision and Pattern Recognition (CVPR) Workshops*, pages 6499–6512, 2024. 2
- [35] René Ranftl, Katrin Lasinger, David Hafner, Konrad Schindler, and Vladlen Koltun. Towards robust monocular depth estimation: Mixing datasets for zero-shot cross-dataset transfer. *IEEE transactions on pattern analysis and machine intelligence*, 44(03):1623–1637, 2020. 1, 2, 3, 4, 5, 6
- [36] René Ranftl, Alexey Bochkovskiy, and Vladlen Koltun. Vision transformers for dense prediction. In *Proceedings of the IEEE/CVF International Conference on Computer Vision (ICCV)*, pages 12179–12188, 2021. 1, 2, 3, 4, 5, 6, 7, 8
- [37] Franco Scarselli, Marco Gori, Ah Chung Tsoi, Markus Hagenbuchner, and Gabriele Monfardini. The graph neural network model. *IEEE Transactions on Neural Networks and Learning Systems*, 20(1):61–80, 2009. 2, 3, 4, 6, 1
- [38] Akash Deep Singh, Yunhao Ba, Ankur Sarker, Howard Zhang, Achuta Kadambi, Stefano Soatto, Mani Srivastava, and Alex Wong. Depth estimation from camera image and mmwave radar point cloud. In *Proceedings of the IEEE/CVF Conference on Computer Vision and Pattern Recognition (CVPR)*, pages 9275–9285, 2023. 1, 2, 3, 4, 5, 6, 7, 8
- [39] Tieshuai Song, Bin Yang, Jun Wang, Guidong He, Zhao Dong, and Fengjun Zhong. mmwave radar and image fusion for depth completion: a two-stage fusion network. In *The 27th International Conference on Information Fusion (FUSION)*, 2024. 1, 2, 3, 4, 5, 6
- [40] Christian Stetco, Barnaba Ubezio, Stephan Mühlbacher-Karrer, and Hubert Zangl. Radar sensors in collaborative robotics: Fast simulation and experimental validation. In *2020 IEEE International Conference on Robotics and Automation (ICRA)*, pages 10452–10458. IEEE, 2020. 1, 2
- [41] Huawei Sun, Hao Feng, Julius Ott, Lorenzo Servadei, and Robert Wille. Cafnet: A confidence-driven framework for radar camera depth estimation. *arXiv preprint arXiv:2407.00697*, 2024. 1, 2, 3, 4, 5, 6, 7
- [42] Hugues Thomas, Charles R Qi, Jean-Emmanuel Deschaud, Beatriz Marcotegui, François Goulette, and Leonidas J Guibas. Kpconv: Flexible and deformable convolution for point clouds. In *Proceedings of the IEEE/CVF International Conference on Computer Vision (ICCV)*, pages 6411–6420, 2019. 2, 3, 4, 8
- [43] Ashish Vaswani, Noam Shazeer, Niki Parmar, Jakob Uszkoreit, Llion Jones, Aidan N Gomez, Łukasz Kaiser, and Illia Polosukhin. Attention is all you need. In *Advances in neural information processing systems*, 2017. 4, 2
- [44] Runzhong Wang, Junchi Yan, and Xiaokang Yang. Learning combinatorial embedding networks for deep graph matching. In *Proceedings of the IEEE/CVF International Conference on Computer Vision (ICCV)*, pages 3056–3065, 2019. 2, 3, 4

- [45] Runzhong Wang, Junchi Yan, and Xiaokang Yang. Learning combinatorial embedding networks for deep graph matching. In *Proceedings of the IEEE/CVF International Conference on Computer Vision (ICCV)*, pages 3056–3065, 2019. 3, 4
- [46] Yue Wang, Yongbin Sun, Ziwei Liu, Sanjay E Sarma, Michael M Bronstein, and Justin M Solomon. Dynamic graph cnn for learning on point clouds. *ACM Transactions on Graphics (TOG)*, 38(5), 2019. 2, 3, 4, 8, 1
- [47] Yiran Wang, Xingyi Li, Min Shi, Ke Xian, and Zhiguo Cao. Knowledge distillation for fast and accurate monocular depth estimation on mobile devices. In *Proceedings of the IEEE/CVF Conference on Computer Vision and Pattern Recognition (CVPR) Workshops*, pages 2457–2465, 2021. 2
- [48] Yiran Wang, Zhiyu Pan, Xingyi Li, Zhiguo Cao, Ke Xian, and Jianming Zhang. Less is more: Consistent video depth estimation with masked frames modeling. In *Proceedings of the 30th ACM International Conference on Multimedia*, page 6347–6358, New York, NY, USA, 2022. Association for Computing Machinery. 2
- [49] Yiran Wang, Min Shi, Jiaqi Li, Zihao Huang, Zhiguo Cao, Jianming Zhang, Ke Xian, and Guosheng Lin. Neural video depth stabilizer. In *Proceedings of the IEEE/CVF International Conference on Computer Vision (ICCV)*, pages 9466–9476, 2023. 2
- [50] Yiran Wang, Min Shi, Jiaqi Li, Chaoyi Hong, Zihao Huang, Juewen Peng, Zhiguo Cao, Jianming Zhang, Ke Xian, and Guosheng Lin. Nvds⁺: Towards efficient and versatile neural stabilizer for video depth estimation. *IEEE transactions on pattern analysis and machine intelligence*, pages 1–18, 2024. 1
- [51] Enze Xie, Wenhai Wang, Zhiding Yu, Anima Anandkumar, Jose M Alvarez, and Ping Luo. Segformer: Simple and efficient design for semantic segmentation with transformers. 34:12077–12090, 2021. 2, 4
- [52] Lihe Yang, Bingyi Kang, Zilong Huang, Zhen Zhao, Xiaogang Xu, Jiashi Feng, and Hengshuang Zhao. Depth anything v2. *arXiv preprint arXiv:2406.09414*, 2024. 1, 2, 4, 5, 6, 7, 8, 3
- [53] Junrui Zhang, Jiaqi Li, Yachuan Huang, Yiran Wang, Jinghong Zheng, Liao Shen, and Zhiguo Cao. Towards robust monocular depth estimation in non-lambertian surfaces, 2024. 5
- [54] Yi Zhou, Lulu Liu, Haocheng Zhao, Miguel López-Benítez, Limin Yu, and Yutao Yue. Towards deep radar perception for autonomous driving: Datasets, methods, and challenges. *Sensors*, 22(11):4208, 2022. 1, 2